ARTICLE

THE ANALYST
www.rsc.org/analyst

Fast automatic registration of images using the phase of a complex wavelet transform: application to proteome gels

Andrew M. Woodward,[a] Jem J. Rowland[b] and Douglas B. Kell†*[a]

[a] *Institute of Biological Sciences, Cledwyn Building, University of Wales, Aberystwyth, Ceredigion, UK SY23 3DD*

[b] *Dept. of Computer Science, University of Wales, Aberystwyth, Ceredigion, UK SY23 3DB. E-mail: azw@aber.ac.uk. E-mail: jjr@aber.ac.uk. E-mail: dbk@umist.ac.uk; http://dbk.ch.umist.ac.uk/*

Received 1st March 2004, Accepted 6th April 2004
First published as an Advance Article on the web 28th April 2004

Image registration describes the process of manipulating a distorted version of an image such that its pixels overlay the equivalent pixels in a clean, master or reference image. The need for it has assumed particular prominence in the analysis of images of electrophoretic gels used in the analysis of protein expression levels in living cells, but also has fundamental applications in most other areas of image analysis. Much of the positional information of a data feature is carried in the phase of a complex transform, so a complex transform allows explicit specification of the phase, and hence of the position of features in the image. Registration of a test gel to a reference gel is achieved by using a multiresolution movement map derived from the phase of a complex wavelet transform (the Q-shift wavelet transform) to dictate the warping directly *via* movement of the nodes of a Delaunay-triangulated mesh of points. This warping map is then applied to the original untransformed image such that the absolute magnitude of the spots remains unchanged. The technique is general to any type of image. Results are presented for a simple computer simulated gel, a simple real gel registration between similar "clean" gels with local warping vectors distributed about one main direction, a hard problem between a reference gel and a "dirty" test gel with multi-directional warping vectors and many artifacts, and some typical gels of present interest in post-genomic biology. The method compares favourably with others, since it is computationally rapid, effective and entirely automatic.

Introduction and background

Proteomics and 2D gel technologies

There is a large and growing increase in the use of modern 2D electrophoretic gel technology ('proteomics') for the purposes of functional genomics (see *e.g.*Link,[1] Mann,[2] Aebersold,[3] and refs. therein).

Whilst mass spectrometry is the premier technology for identifying specific proteins from such gels,[4,5] comparative proteomics, in which the same organism or type of extract is studied under different conditions, relies solely on comparisons between images in which 2D gels are stained with silver stain, a chromophore such as Coomassie Blue, or fluorimetrically.[6] Inevitably, such gels are less than perfectly reproducible, and the image data obtained by an instrument from successive gels of even the same sample will differ, due to calibration drift (see refs. 7–11) of the electrophoresis equipment, changes in the exact experimental conditions, and so on. For different samples there will of course be the more interesting and genuine changes in spot intensities in the gels. In consequence, it is necessary to align any new gel to make it concordant with a similar reference gel, so that all the spots from identical proteins are in the same places. Relative intensities can then be compared, while new spots which are not present in the reference gel (or alternatively species that are missing from the new gel) can be detected and if appropriate identified.

Note that although 2 or 3 proteomes may be compared within the same gel by dual- or triple-labelling, and with multispectral imaging,[6,12,13] this still does not solve the problem of irreproducibility between days.

Image registration establishes the correspondence between two images and determines a method of aligning them with each other. It is the process of manipulating a new (test) image to match a reference image by correcting spatial distortions and misalignments in the test image. Gel analysts commonly do this manually by visually or semi-automatically identifying significant equivalent spots ("landmarks" or "control points") in both gels, selecting them manually, and then comparing the reference with the test gel so that these spots are matched against the chosen equivalents in the reference gel. This is the only method available in most of the commercial and other proteome software such as Phoretix, Melanie, PDQuest, Flicker and the like, and it is both very time consuming, completely subjective (as it depends on which landmarks and thresholds are chosen), and subject to error.[11]

Existing methods for automating image registration

Several broad categories of approach have been used in attempts to automate the process of image registration. These often come from video processing research, from medical scanning or astronomy, but most deal only with images which are simply translated, rotated and/or linearly stretched. These methods include grey-scale histogram analysis,[14–19] texture analysis,[20,21] edge enhancement and linking,[16,20–25] region growing,[20,26,27] contour following,[16,21,23,25,28] and the maximisation of spatial correlation or mutual information between images.[18,29–37]

Landmark-based methods rely on marking and aligning easily identifiable point features,[15,18,38,39] and manual landmarking is one of the main methods used in the commercial proteome software. Segmentation methods divide the picture up into areas or 'segments', often by contour following, or by region growing and the related watershed methods,[40–44] which can then be moved for image alignment.[18,20] Deformable models (rubber-sheeting) can be used in conjunction with both methods to warp the test image to the reference.[45–49]

An ideal gel registration method would deal with general warping functions and multi-directional warping vectors, and would be completely automatic. It would also be able to preserve additional or missing gel spots in the test image, since these small differences are often the most significant factor in the subsequent

† Present address: Dept. Chemistry, UMIST, Faraday Building, Sackville St, PO Box 88, MANCHESTER M60 1QD. E-mail: dbk@umist.ac.uk, website: http://dbk.ch.umist.ac.uk/, Tel: 0161 200 4492

DOI: 10.1039/b403134b

analysis of the registered gels. Since the spatial differences between the 'same' spots on different gels depend on where the spots are located, the registration process must be able to cope with both global and local deformations in the test image.

Since the spatial differences between the 'same' spots on different gels depend on where the spots are located, the registration process must be able to cope with both global and local deformations in the test image. Gustafsson and colleagues[9] used a 2-stage warp, the first of which involved a model of current leakage during the electrophoresis (which may be restrictive to that model) and the second a bilinear, multiresolution, gradient descent algorithm, while Smilansky[10] used a 'shift vector list' approach for the gel warping problem, and also studied visualisation issues. Veeser *et al.*[11] described an approach using a gradient descent algorithm to dictate the warping of a multiresolution grid across the image in *x*-*y* to optimise a cross-correlation-based distance metric formed on the local image area. We (unpublished) and others (*e.g.* refs. 50–52) have developed one-step registration methods using Genetic Algorithms that produces excellent robust registration but at the cost of the computational intensity associated with evolutionary programming methods. The research presented here develops on that work by presenting a much faster method, which is deterministic instead of heuristic, using the phase of a recently developed complex wavelet transform[53–65] to dictate the movement map. The basic idea is that intensities are largely encoded in the real part of the complex wavelet transform while position is largely encoded in the phase. Registration might then be achieved by adjusting the phase of a test gel to reflect that of a reference gel. Sub-pixel precision is achieved because the movement at each point in the image is derived from an extrapolation of a phase difference not from a direct pixel comparison.

Loo and Kingsbury[66–68] have applied the complex wavelet transform to watermarking, which is a similar problem to image registration. Our method modifies this approach, speeding up the calculations such as to make registration of gel images a viable prospect on a desktop PC.

The fast complex wavelet transform

Since the spatial differences between the 'same' spots on different gels depend on where the spots are located, the registration process must be able to cope with both global and local deformations in the test image. Multiresolution methods such as the wavelet transform (*e.g.* refs. 69–75) allow this to be achieved, by simultaneously operating on several scales at once.

Wavelet transforms give a measure of the correlation between the image and a chosen "mother wavelet" function. This wavelet is stretched, moved, and the correlation determined for each dilatation and position. This stretching of the wavelet allows study at multiple scales. Long wavelets highlight large-scale features in the image and short wavelets highlight small-scale features. The summation of all scales in the wavelet transform allows a very versatile and powerful multiresolution representation of the image.[69] If special orthonormal wavelets are chosen, then the transform can be perfectly inverted to reconstitute the original data in the same way as the well known Fourier transform. The significant advantage of the wavelet transform over the Fourier is that whereas the sinusoidal base-functions of the Fourier transform are infinite in length, wavelets are finite, and so allow the transform to contain information about local features in the data, such as spots in proteome gels.

A novel approach to robust, automated image registration

The fast wavelet transform has a severe drawback for this particular application. This is its shift variance, such that a small displacement of the signal can make large differences to the distribution of its wavelet coefficients. Since registering gels (and images in general) usually requires the removal of small displacements, this problem becomes severely limiting. The reason for this shift variance is that even with ideal perfect wavelets in a dyadically down-sampled fast transform, the Nyquist criterion would only barely be satisfied at each scale, and with practically realisable wavelets the data are under-sampled.[57,76]

The continuous wavelet transform[77,78] on the other hand is shift-invariant. However, this transform is massively redundant, slow and not invertible and thus not suitable for practical analysis of large images.

In this paper, we produce a rubber sheeting method of registration, applied using a multiresolution approach and controlled by a movement map produced by a shift invariant wavelet transform. This allows the correction of arbitrary displacements of gel spots and areas, with arbitrary linkage between the corrections to be applied at each level, instead of the global corrections of simple translation, rotation and linear warping achieved by current automatic registration routines. Specifically, we achieve the identification and implementation of the vector corrections needed to produce the movement map using phase-manipulation of a newly developed complex wavelet transform.[62–64] Importantly, the complex nature of the wavelet coefficients in the complex wavelet transform introduces a double redundancy into the wavelet representation. Hence the amplitudes of the complex wavelet transform coefficients are shift-invariant; and the phase is linearly variant with shift, and locally referenced within the scope of each individual wavelet coefficient.[57,59,60] Whilst other wavelet transforms exhibit shift-invariance, they do not exhibit the unique combination of reconstruction, orthogonality, redundancy, locality and linearity which is what gives this new transform the required capabilities for image registration.

Exploitation and parameterisation of the complex wavelet transform for automated image registration

Much of a data feature's positional information is carried in the phase of a complex transform,[79] so a complex transform allows explicit specification of the phase, and hence of the *position* of features in the image. Phase differences between warped but otherwise identical images give information about the relative movement of regions of the images.[62–64] The coefficients of Fourier-based transforms store the sequence information globally, whereas convolution based transforms such as the various wavelet transforms store information locally. In a multiresolution representation, then, all scales of movement can be specified, from largest scale mass movements to tiny regional warpings.

The structure of a complex wavelet transform can be as simple as that of the discrete wavelet transform using the Mallat Algorithm,[74] except that the complex filters require complex coefficients and generate complex output samples. Unfortunately it is very difficult to obtain perfect reconstruction and good frequency characteristics using short support complex FIR filters in a single tree. Kingsbury[53,59] introduces the dual tree complex wavelet transform which adds perfect reconstruction to the other attractive properties of complex wavelet: shift invariance, good directional selectivity, double redundancy, and efficient order-*N* computation.

The structure of the Fast Dual Tree Wavelet Complex Transform (DTWT.) uses two separate Mallat algorithm trees[53,59] in parallel as in Fig. 1.

However, when the outputs from the two trees are interpreted as the real and imaginary parts of complex wavelet coefficients, the transform effectively becomes complex. To invert the transform, the perfect reconstruction filters *G* with the corresponding analysis filters *H* are applied in the usual way to invert each tree separately, and finally the two results are averaged, which is shown lower right in Fig. 1.

A later development of the dual tree wavelet transform, called the Q-shift transform (QSWT), has been proposed to make the sub-sampling structure symmetrical.[59–61] The differences mainly focus on the filter design and the relative sampling delay of each tree at each level.

Extension of the DTWT and QSWT to two dimensions is easily achieved by separable filtering along columns and then rows, with 4:1 redundancy produced in order to represent fully a real 2D signal.

The mathematics of the DTWT has been covered very comprehensively in the references cited[53–67,80] and is not reproduced here. The practical considerations for the non-specialist use of this very useful but not widely known algorithm are stressed instead of its internal details in the hope of increasing its application to the many signal processing fields to which it could be beneficial.

The output of this algorithm at each scale is a set of 6 subimages. Each of these has its own directionality, in which the phase is most sensitive to displacement. The impulse response of each subband and directionality are shown in Fig. 2; and this directionality provides the vital orientation information for creating movement maps.

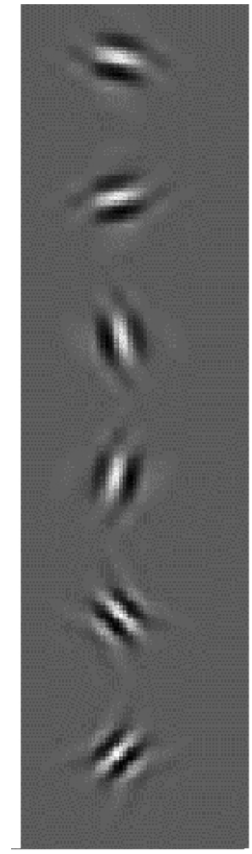

Subband	Angle
1	75
2	-75
3	15
4	-15
5	45
6	-45

Fig. 2 Impulse responses of subbands 1 to 6, showing their directionality. The direction of greatest phase sensitivity is perpendicular to the wavefronts.

The QSWT-warp methodology

For this work, the more uniformly sampled QSWT was used. Tests transforming, filtering, and retransforming particular images showed little difference in utility of the various wavelet filters supplied with the QSWT software.[59–61] Here, the biorthogonal Near-Symmlet-A wavelet was used for the initial stage of the QSWT algorithm, in conjunction with the Q Shift A wavelet for the rest of the algorithm trees.

The conventional way in which the DTWT has been used to date is to form the Squared Difference Surface (SDS) for each pel in each subband at each scale.[62,64] (A pel is the scope of a wavelet coefficient — *i.e.* that area of the image covered by that coefficient at that scale such that at scale m, a pel is $2^m \times 2^m$ pixels). The SDS is a measure of similarity between the current pel in the test image and displaced versions of the reference image, and is formed by a 2D scan of displacements around the centre of the reference pel for each subband, and subsequently summing all these subbands to form a dished surface. The formation of the SDS requires the assumption that for small displacements, the amplitude of a complex pel will remain approximately constant and the phase of the pel will vary linearly with displacement (see ref. 64).

The minimum of the resulting surface gives the best estimate of magnitude and direction for the displacement between the test and reference pels. So computing it for each pel requires a 2D scan,

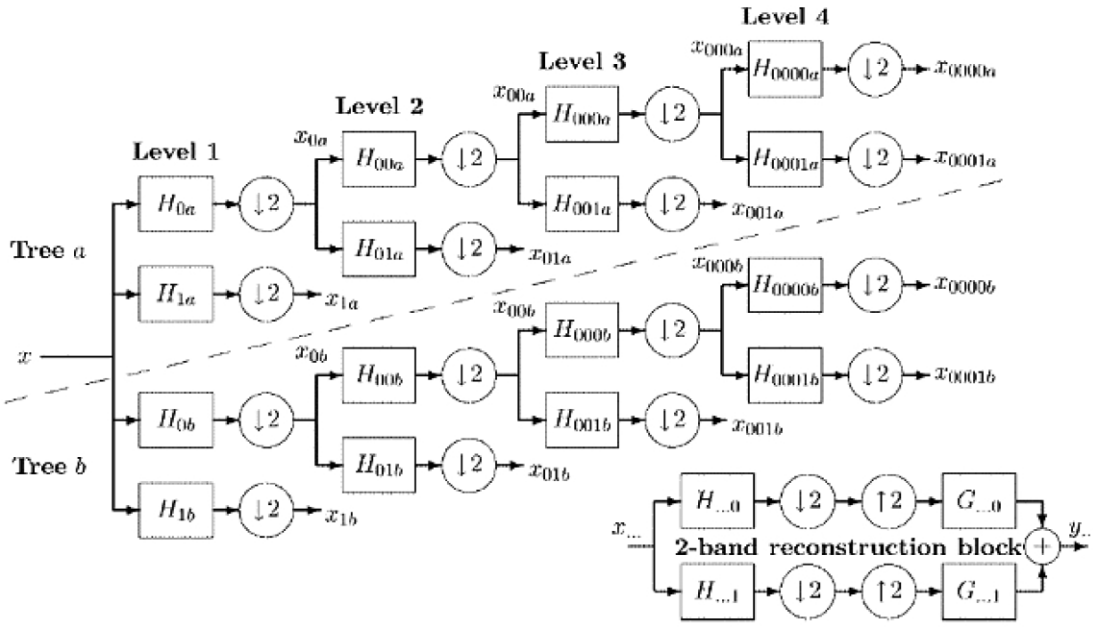

Fig. 1 The Dual Tree Algorithm (DTWT), comprising two trees of real filters, a and b, which produce the real and imaginary parts of the complex coefficients. Figure after ref. 55.

followed by curve fitting to the surface to find the exact minimum position. The sharpness of this minimum in various directions defines the reliability of that distance estimate in that direction.[62,64] Unreliability arises both from the above assumption being violated, and from the phase of tiny coefficients (subject to noise) having as great a phase swing as large clean ones. Phase always varies from $-\pi$ to π no matter how large or small the amplitude of the coefficient; so null areas of an image appear as important to a phase-map as those areas containing significant features. The reliability metric above is used to pick only the most dependable movement estimates and interpolate the complete movement map from these, rejecting unreliable estimates.

This procedure is firstly carried out at the longest scale of the DTWT decomposition to derive the movement map at coarsest resolution, then the results of this are carried through to the next shortest scale, and the procedure repeated hierarchically through to the shortest scale and finest resolution of decomposition.[62,64,66–68]

Observation, and Fig. 7 in ref. 64 and Fig. 3a of ref. 68 suggests that the contours of the SDS for each individual subband are, at least to a very close approximation, straight lines perpendicular to the directionality of that subband, only forming a dished surface when summed with all the other subbands for that pel. The equiphase condition[64] expressed in eqn. (1)

$$2^m(\boldsymbol{\Omega}^{(n,m)})^{\mathrm{T}}\,\boldsymbol{f} = \arg[\mathrm{D}_2^{(n,m)}(n)/\,\mathrm{D}_1^{(n,m)}(n)] \qquad (1)$$

where m = scale, n = subband, D_1 = DTWT reference coefficient, D_2 = DTWT test coefficient n = reference coefficient centre position, $\mathbf{f}$ = movement vector to equiphase position from reference pel centre and $\boldsymbol{\Omega}$ = subband filter centre frequency, in conjunction with the substantially planar nature of the SDS surface for each subband implies that the phase gradient can be simply extrapolated to solve this equation in the direction of that subband in order to produce the projection of the movement for that pel in the direction of that subband. This replaces a 2D scan with a single calculation, giving the projection not only to sub-pel precision, but also to sub-pixel precision. These movement bases for each subband can then be vectorially added for all 6 subbands to produce the overall motion vector for that pel.

The angular frequency of a subband, $\boldsymbol{\Omega}$, can be obtained from the equations for the subband filter. However, non-specialists in filter design can deduce its magnitude for any subband from the standard relationship that $\boldsymbol{\Omega}$ is the rate of change of phase with respect to the independent variable and the experimental observation that movement of a delta function diagonally produces a phase change rate of 2π/pel in the corresponding 45 degree subband. The direction of $\boldsymbol{\Omega}$ can be derived from the knowledge that $\boldsymbol{\Omega}$ in eqn. (1) for a particular subband is the centre frequency of this band and specifies its direction.[64] The distribution of centre frequencies of subbands is represented graphically in Fig. 3.

Thus the scaling vectors of the $\boldsymbol{\Omega}$ values for the subbands is given by the complex vectors to the centre of the filter passbands as in Table 1.

Comparing the movement map produced by the SDS *vs*. that produced by the phase gradient shows the two approaches produce virtually identical vector maps as shown in Fig. 4 for a pair of proteome gels from *Dictyostelium discoides* cultures.[81] However the phase gradient method runs 100 times faster, taking 24 s instead of 2630 s on a P700 PC.

Accordingly the phase gradient method was used to create the movement maps for this paper. These movement maps were then used to control image warping using Matlab.[82]

It should also be noted that the phase differences derived from the equiphase condition above are identical to the phase of a cross complex-wavelet transform between the test and reference images. Computing the phase of the Cross QSWT directly is found to give identical movement maps to solving eqn. (1).

The price paid for this massive decrease in computing intensity is that this procedure does not give a direct measure of reliability but as will be seen in the results later, this is not a requirement in the application discussed here.

It may be thought that registration could be achieved simply by substituting the phase from the reference image into the test image. However, as noted in ref. 79, a phase only reconstruction of an image reconstructs much of the structure of that image, giving a result very similar to simply a high passed original image. So if the phase of the reference image is substituted into the test image, then the resulting image registers the common spots well, but tends to ignore new or missing spots in the test image. Our new phase gradient method avoids this problem by warping the original image rather than a transformed version of it.

A measure of reliability can however be derived using the phase gradient method. The derivation for the Squared Difference Surface and by extension, the equiphase equation above relies on the assumption that each pel has an effectively constant amplitude between reference and test pels and only the phase changes significantly, signifying a simple translation instead of a significantly changed subimage. Also the algorithm may be unstable for wavelet coefficients which are small in both reference and test subimages, in a manner analogous to rounding error. Phase differences between tiny coefficients span the same angular range as those between huge coefficients, so phase does not ignore null parts of the picture.

Thus, reliability could be enhanced by rejecting movement vectors in which both instances of a particular pel amplitude are small, which corresponds to a null part of the image (in our particular application, there are no gel spots in the pel); and also where amplitudes are substantially different signifying that pels are significantly different (one is missing or gaining features compared to the other — in our case gel spots are moving in or out of the scope

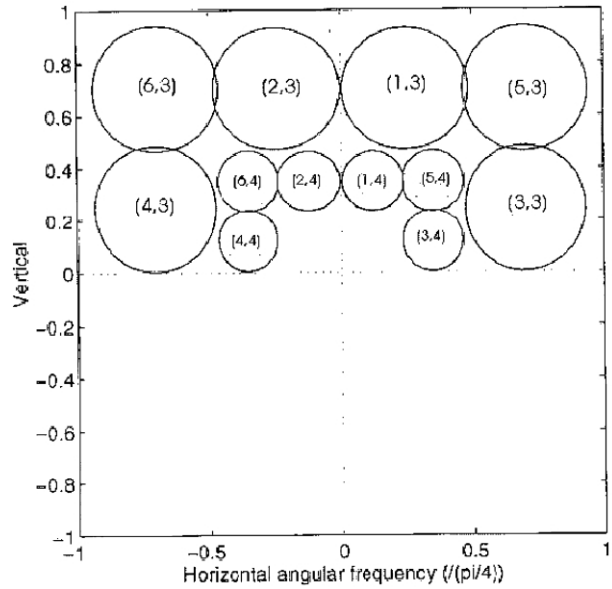

Fig. 3 Passband structure for scales 3 and 4. Subbands are numbered (band,scale). Figure modified slightly for subband numbering after ref. 64.

Table 1 Scaling factors for specifying direction of $\boldsymbol{\Omega}$ for each subband in a scale

Band	Subband scaling factor
1	1/3 + j
2	1/3 − j
3	1 + j/3
4	1 − j/3
5	1 + j
6	1 − j

of the pel such that one is comparing significantly different subimages instead of a simple translation of substantially the same subimage). Phase information is regarded as reliable where both pel amplitudes are fairly similar — both subimages contain similar data and phase information should purely reflect relative movement between the pels.

A simple way to achieve this selection is to map (difference between pel amplitudes)/(mean of pel amplitudes) between the reference and test images to form a mask of movement vectors reflecting pure translation where difference/mean is small. This will give a sparse matrix of WT coefficients which can be interpolated to full coverage.

For the particular case of proteome gel images, pel selection can be further simplified. Registration should only use scales significantly longer than the peak scale — that scale which contains the maximum energy. The gel spots are all of roughly similar size and will therefore fall into a very narrow band of scales, reflected in this peak scale. It is not required to warp the gel on the scale of single spots, since the warping mechanisms operate on a larger scale than the size of single spots. Colloquially, we don't want to move bits of spots, only areas of them. In addition, with something like a gel, where the features are concentrated around a narrow band of scales, it is vital *not* to match longer scales since these will reflect variations of spurious baseline background features rather than gel spots, so the movement vector maps associated with these scales will be wrong. Thus, at least the longest two scales, and the shortest down to at least one scale longer than the peak scale, can be rejected without further consideration.

Registration can be improved by removing the baselines from the gel images in a prior preprocessing step, however the longest scales of the wavelet transform still do not significantly contribute to the registration. A suitable baseline removal method for proteome gels is to form a 2D moving median average over the gel using a sufficiently large footprint as to be significantly larger than twice the largest gel spot. This will select the baseline and remove all spots as outliers (exactly analogous to image despiking). Simply subtracting this result from the gel image would subtract the baseline and leave the spots sticking up from a flat background, since in proteome gels, the "outliers" are the required signal.

However, when applied to gel images, intra-scale pel selection as above was found to make little difference to the Minkowski distance between images, and no visual difference, merely introducing extra parameters. Thus we conclude that, at least in gel registration problems, the cross spectral method of forming movement maps is robust to error within each scale and doesn't need any special effort to differentiate between the reliability of different subband coefficients This can be seen in the quality of registrations presented later which were produced without any form of pel selection other than baseline removal and then simply rejecting the longest two and shortest three scales from the wavelet transform.

The Matlab image warping algorithm from the Matlab Image Processing Toolbox V.3[83] requires the setting of control points in the test image and of 2D displacements by which these control points are to be moved. These control points are then Delaunay triangulated[84,85] into a piecewise linear approximated surface and the movement of the vertices of this surface dictate the warping of the image.

We choose to impose a rectangular mesh on the image at each successive iteration. Virtual control points are chosen to be the vertices of this mesh, and are placed at the centre point of each pel at that scale. The *x*-*y* displacements of these vertices are generated by the *x* and *y* components of the sum of all the subband movements of each pel at that scale

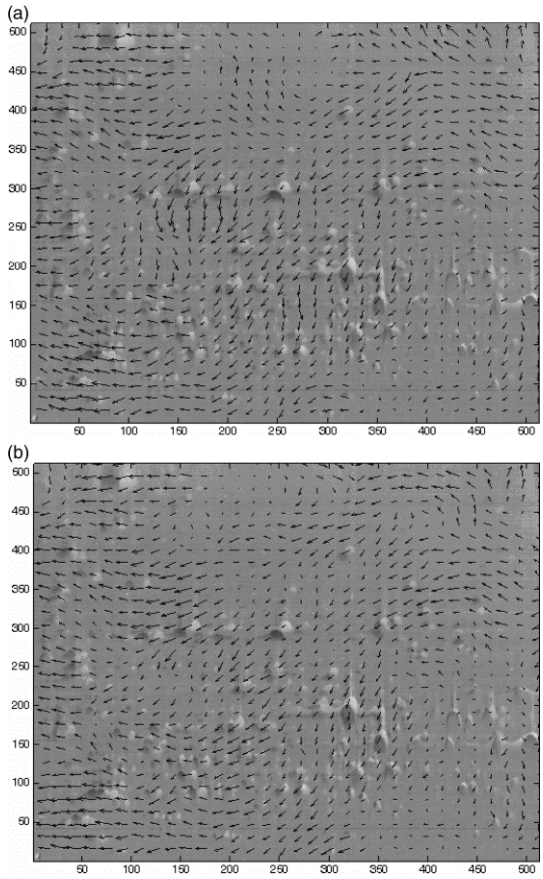

Fig. 4 Phase gradient movement map derivation *vs.* the standard Squared Difference Surface method. The figures show the difference between reference and test gels, gels from *Dictyostelium discoides*, such that the warping between the two shows up as black/white doublets. The motion vector arrows derived from the complex wavelet transform can be seen to reflect the magnitude and direction of the doublets very well.

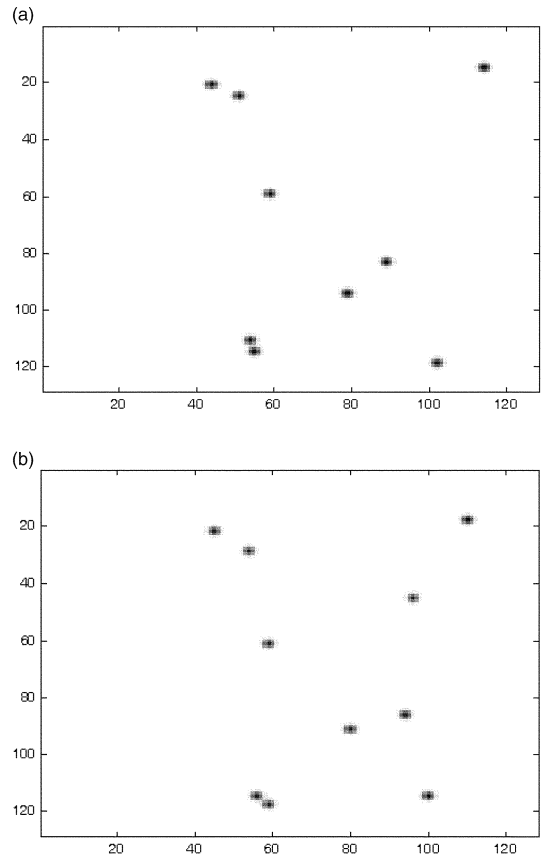

Fig. 5 Simple computer simulated reference and test gels for algorithm development. The Euclidean distance between these gels is 6.7.

A metric of similarity

Similarity between images can be judged by any of the current methods for computing multivariate distances between the images[86–90] for determining and subsequently adaptively (intelligently) controlling the degree of transformation applied to the test image in the registration process. Removal from the images of noise and background levels must be done prior to this step.

However, our unpublished observations showed that a simple pixelwise Minkowski Distance with radix two,[89,90] equivalent to a Euclidean distance, with each pixel representing a dimension/variable was almost as accurate as any more complicated alternative and is computationally very simple and quick.

Pel selection for proteome gels

Proteome gel images have certain features that make them simpler to analyse than general images. They are a distribution of somewhat similar sized spots superimposed on a background which should possibly be, but for many reasons (*e.g.* ref. 12) in practice rarely is, null. The longest scales hold information on the background and tend to comprise only low amplitude coefficients. The shortest scales hold information on the spots themselves, and those in between hold information on the warping field of the gel. So after the background has been removed by other means as a preprocessing step, then most of the energy in the DTWT will be concentrated in the shortest few scales, which represent the spots.

For registration, only scales longer than the peak scale (in terms of energy contained per scale) should be used, since the peak scale contains information on spots, and gel warping occurs at scales longer than individual spot sizes (spots retain their relative positions but move their absolute positions). Consequently, for the purpose of forming a movement map, the longest and shortest scales can be rejected as a form of denoising. Registration is carried out using those remaining scales reflecting the scale of warping of the images.

As stated above, the phase gradient method does not give a reliability estimate for each pel within a scale, but this can be obtained by rejecting small coefficients (which are unduly subject to noise problems) and also by rejecting those in which the amplitude changes significantly (which violate the assumptions used to derive the equiphase equation). Constant amplitude pels between the reference and test image signify that only movement is occurring between those pels. Changing amplitude implies that features are moving in or out of the pel scope. However, experiments show that the phase gradient algorithm is sufficiently robust that this intra-scale pel selection is not needed, at least in the task of registering proteome gels. It makes negligible difference to the results presented below although its inclusion does not significantly slow the algorithm down either.

We would wish to stress that no user input is thus required, either in setting control points or in the optimisation of their displacement.

Results

Simulated gels

Initially the method was proved on simple computer simulated gels consisting of 10 Gaussian spots randomly placed on a flat zero background 128 × 128 pixels in size. The test gel was constructed by moving the spots of the reference gel randomly by up to ten pixels and adding another spot at pixel (45,96) to simulate a real difference in proteome between the gels, as shown in Fig. 5.

Any registration algorithm must be able both to align the spots existing in both gels while maintaining the information contained in extra (or missing) spots in the test gel. In other words it must

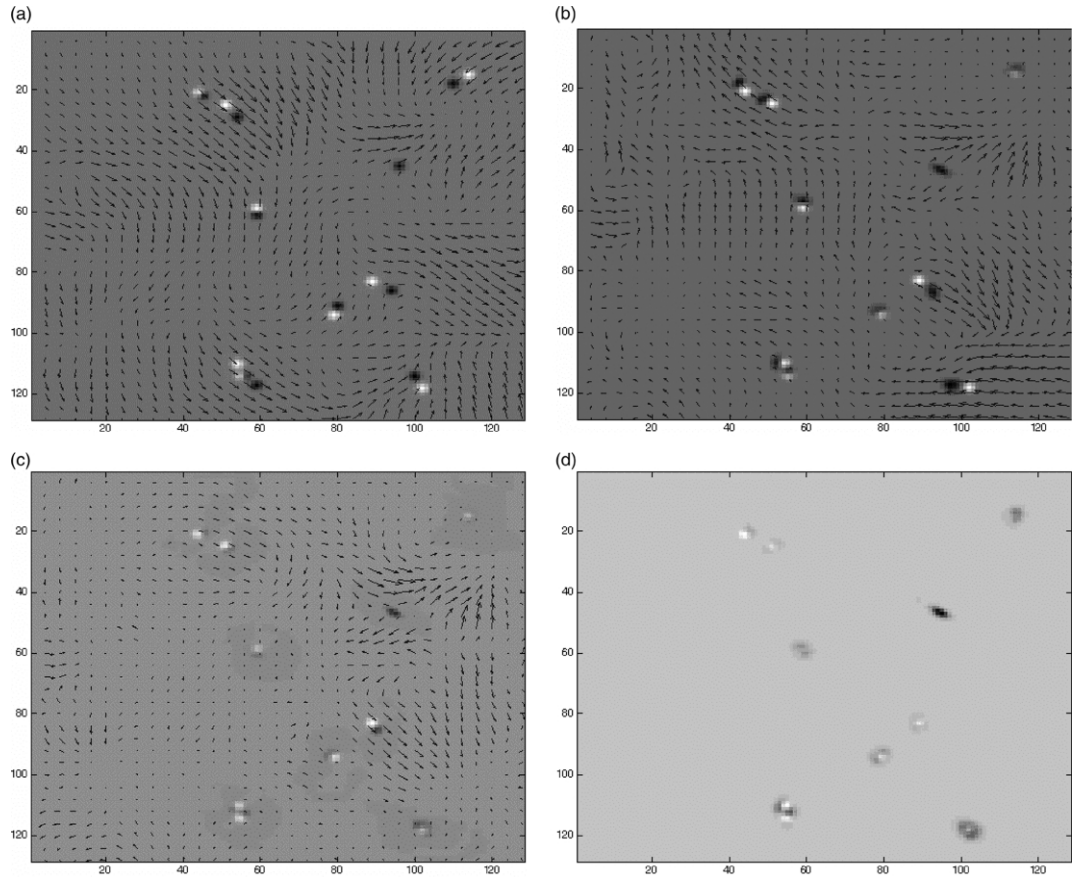

Fig. 6 Progression of iterative registration of computer simulated gels by the phase gradient method. (A) Difference of original gels with first iteration warping field superimposed. Euclidean distance between gels is 6.7. (B) Stage 1 registration with second iteration warping field superimposed. Euclidean distance is now 5.9. (C) Stage 2 registration with third iteration warping field superimposed. Euclidean distance is now 4.0. (D) Final registration. Euclidean distance is now 2.4.

eliminate spurious differences between gels (warping) but maintain real differences (different proteome structure). Computer simulated gels like these make it much easier to show the effect of the transformation on the vital missing or extra spots between the gels. Real (*i.e.* experimentally acquired) gels are often so complicated that it can be difficult to discern what is happening to (often very faint) missing or extra spots. When the functionality of the method is proved on such testbed images, it can be applied to real gels. These computer-simulated gels purposely represent a controlled but very difficult registration problem, with large, randomly orientated and independent displacement of each individual spot. In real gels the spot movement is much smaller and the warping varies relatively slowly over the area of the gel with areas of spots locally correlated in their displacements.

As stated above, with something like a gel where the features are concentrated around a narrow band of scales, it is vital not to match longer scales, since these will reflect variations of background

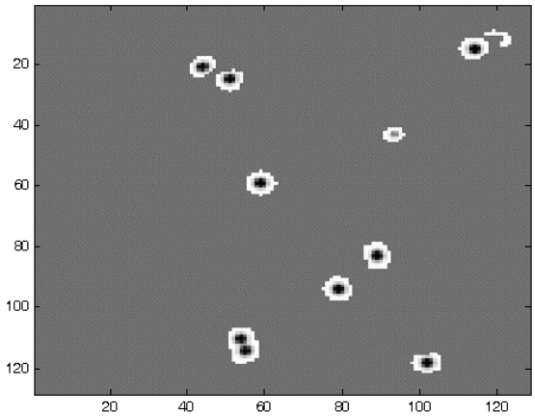

Fig. 7 Registration of the test and reference gels in Fig 5, using the MIR method.[11]

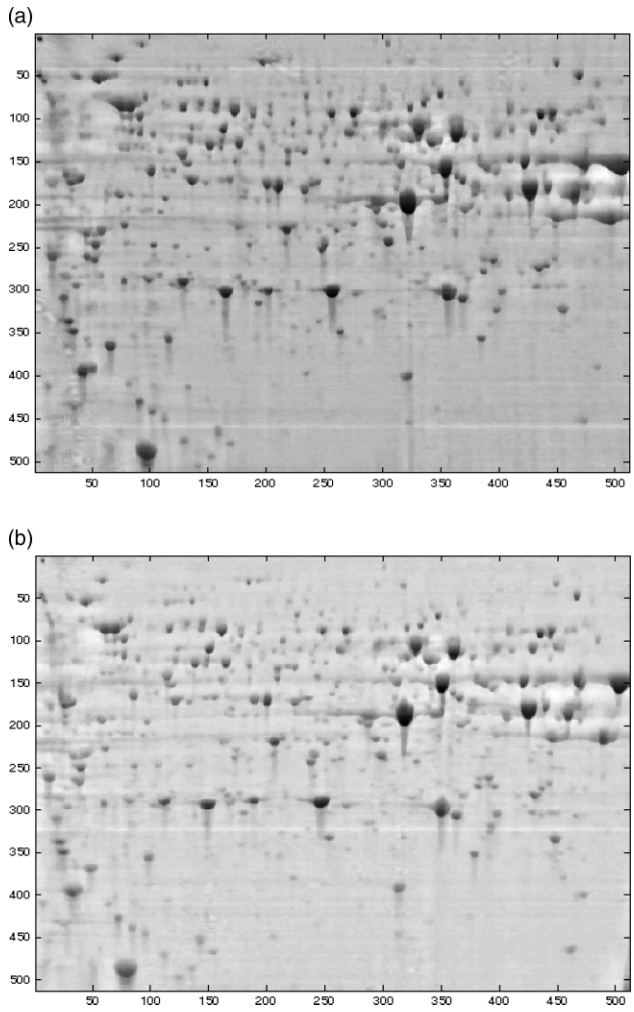

Fig. 8 *Dictyostelium discoides* gel images: Reference gel is control culture. Test gel is culture previously exposed to an electromagnetic field. The Euclidean distance between the gels is 260.

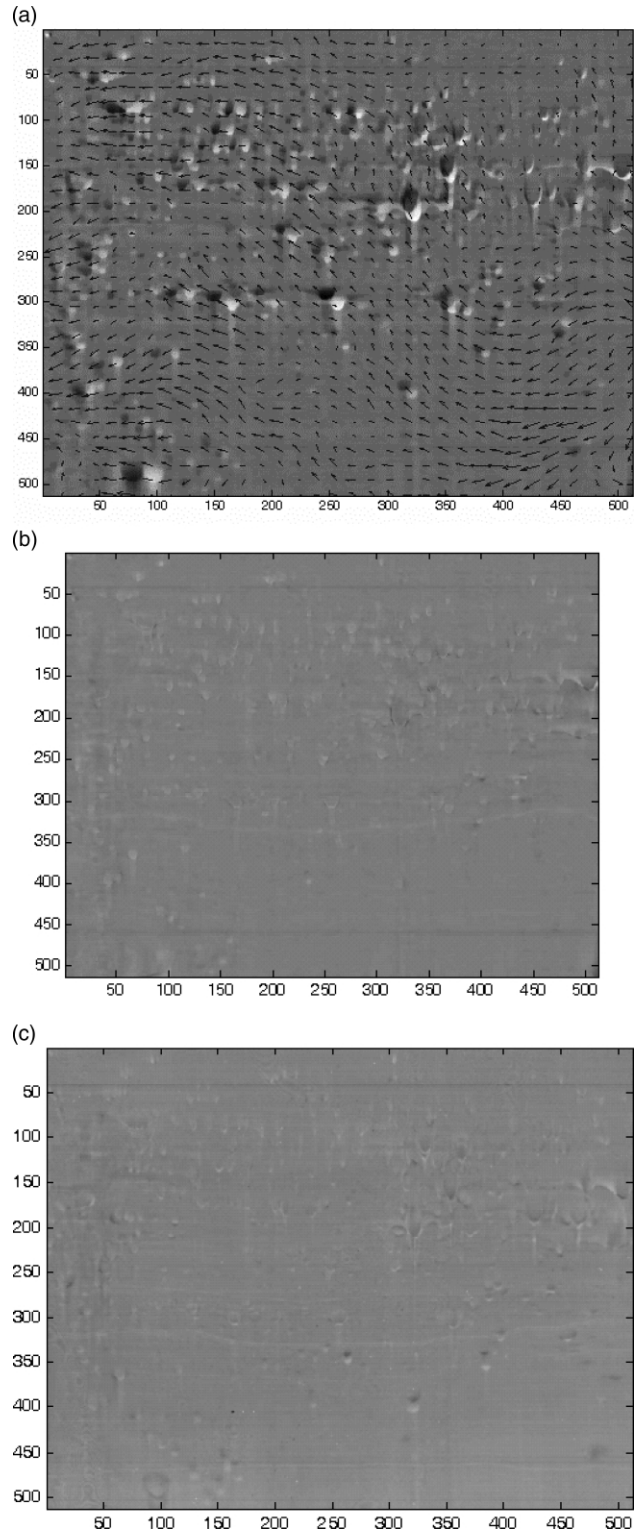

Fig. 9 Iterative registration of *Dictyostelium discoides* gel images. A and B use the QSWT phase gradient method, C the MIR-method. (A) Difference of original gels with first iteration warping field superimposed. Euclidean distance between gels is 260. (B) Final (4th iteration) registration. The Euclidean distance is now 127, *i.e.* a ratio of 1:0.48. (C) Registration of the same gels using the MIR method: the ratio of the Euclidean distances before and after registration is 1:0.87.

features rather than gel spots, so the movement vector maps associated with these scales will be wrong. The shortest scales also don't reflect the gel spot movement field, and their inclusion is found to makes no difference at all to the Euclidean distance of the registered gel. So the heuristic is, at the initial iteration, to subtract longest scales till minimum Euclidean distance, then subtract shorter scales till Euclidean distance increases. The phase gradient algorithm is easily fast enough to allow this. From then on, the longest remaining scale is removed at each successive iteration till only one scale remains.

Magarey and Kingsbury[62,64] using the SDS method, form the movement map at the longest scale, then uses the result of this as the starting point for the map at the next shortest scale and so on. The speed of the phase gradient algorithm allows a multiscale resolution at each iteration, starting with full registration using the all optimum scales to form the movement map as above, then retransform and construct a multiscale partially registered image. This can now be used as the base image for repeating the procedure with another multiscale decomposition, which now no longer needs the longest scale used previously since large scale movements have been removed by the previous iteration, continuing till only the finest significant scale is left.

Warping uses a scale-dependent mesh such that reconstructions including long scales use coarser mesh than those later reconstructions using only shorter scales. Previous large scales will have already removed large displacements, so we can use finer mesh for better registration of fine detail. Warping mesh intersections are placed at the pel centre for each scale.

For these computer simulated gels, scales 1 and 2 hold no information on the movement field, and do not affect the registration at all; while scales above 6 contain only small amplitude coefficients and are rejected also. So in only 3 iterations, registration is very good.

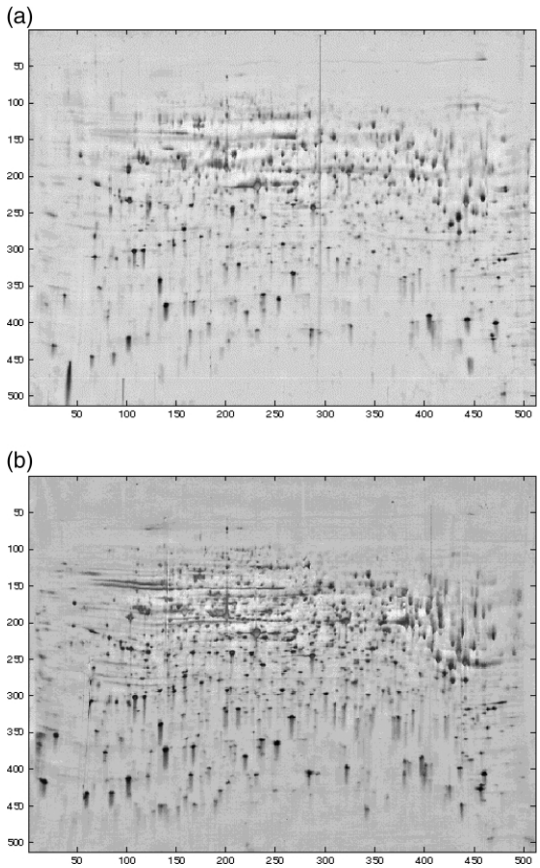

Fig. 10 *Caenorhabditis elegans* gel images. The Euclidean distance between the gels is 259.

As in Fig. 1, the degree of registration throughout this work is represented by the difference between the reference image and the image at that stage of registration. Mismatched spots show as dark/light doublets — the spacing and direction of these doublets showing the magnitude and direction of the remaining registration field required

The difference between the reference and original test gel, together with the movement map created by stage one of the phase gradient iteration using scales 5,4,3, is shown in Fig. 6a. The movement map at this iteration can be seen to follow the mismatched doublets quite well. Fig. 6b shows the next iteration with the stage two movement map using scales 4,3 superimposed upon the stage 1 registration. Fig. 6c shows the third iteration movement map using scale 3 superimposed upon the second stage registration, and Fig. 6d shows the final registration.

11 further iterations using scale 3 can reduce the Euclidean distance down to a minimum of 2.1 with no visual improvement.

Note that all the doublets denoting mismatched spots in Fig. 6a have been resolved very well (they should ideally disappear), and that the integrity of the extra spot in the test gel has been preserved.

We compared these registrations of the synthetic gel image with the MIR algorithm published by Veeser,[11] using the program they produced for this available at http://vip.doc.ic.ac.uk/2d-gel/GelRegister.exe. The basis of their algorithm is a hierarchical gradient search optimisation of a three scale multiresolution grid.

The most obvious difference between MIR (Fig. 7)and the present one is that the shape of the spots is significantly distorted

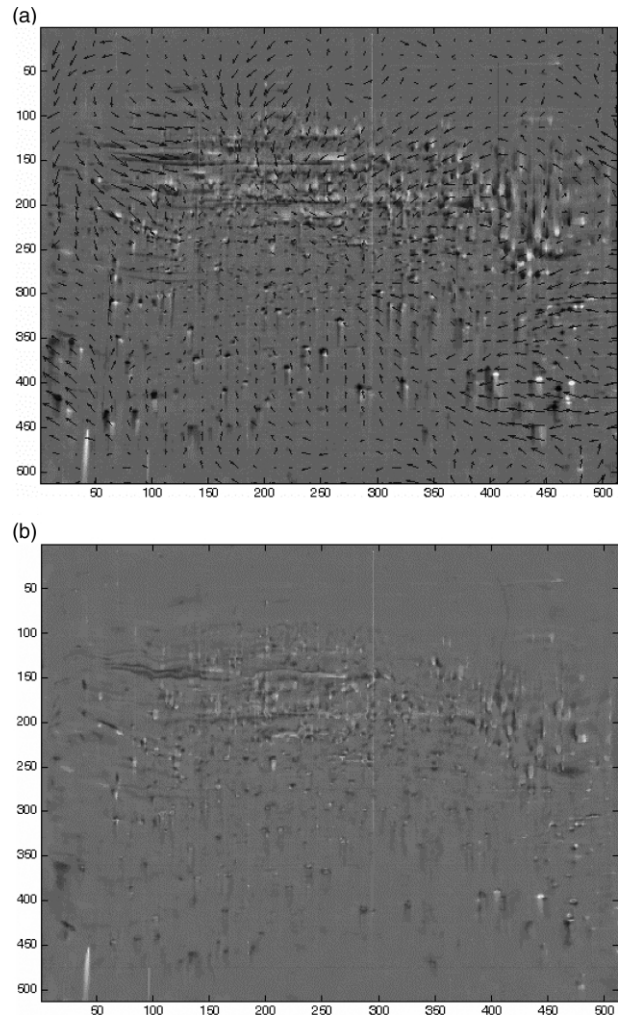

Fig. 11 Iterative registration of *Caenorhabditis elegans* gel images by the phase gradient method. (A) Difference of original gels with first iteration warping field superimposed. Euclidean distance between gels is 870. (B) Final (4th iteration) registration. Euclidean distance is now 181.

(and an artefact is visble in the top right hand corner). However the registration is good in positional terms. The Euclidean distance between the MIR-registered and the reference gel (as normalised to an unregistered distance of 1) is 1.83, so the distortion of the spots has apparently increased the overall Euclidean distance. The times required for the registration were comparable (7s for MIR method, 5s for the QSWT).

Dictyostelium discoides

Having proved the efficacy of the GA registration method on simulated gels, a pair of proteome gels from *Dictyostelium discoides*[81] were registered.

Before registration it is beneficial to remove the background baselines due to non-uniform illumination of the images. The baselines are first removed from the images by scanning a 2D median filter of length and width significantly greater than twice the largest spot diameter across the image in order to derive the baseline by filtering off the spots; and then subtracting this baseline from the image. The resulting gel-images are shown in Fig. 8.

The mismatch between these two gels is predominantly distributed around a dc shift, as can be seen in Fig. 8a.

Using the same procedure as for the synthetic gels produced a similar registration sequence. The difference between the reference and original test gel together with the movement map created by stage one of the phase gradient iteration, using scales 6,5,4,3 is shown in Fig. 9a. Again, the movement map at this iteration can be seen to follow the mismatched doublets quite well. Further iterations take the Euclidean Distance down through 191, 152, and 132 to produce the excellent final registration shown in Fig. 9b. The equivalent registration using the MIR method is shown in Fig 9c. The registration is good save for 3 unmatched doublets in the lower center right. In this case the MIR method is slightly faster (8s *vs.* 25s), though we note that the MIR method is compiled while the QSWT method implemented in Matlab is interpreted.

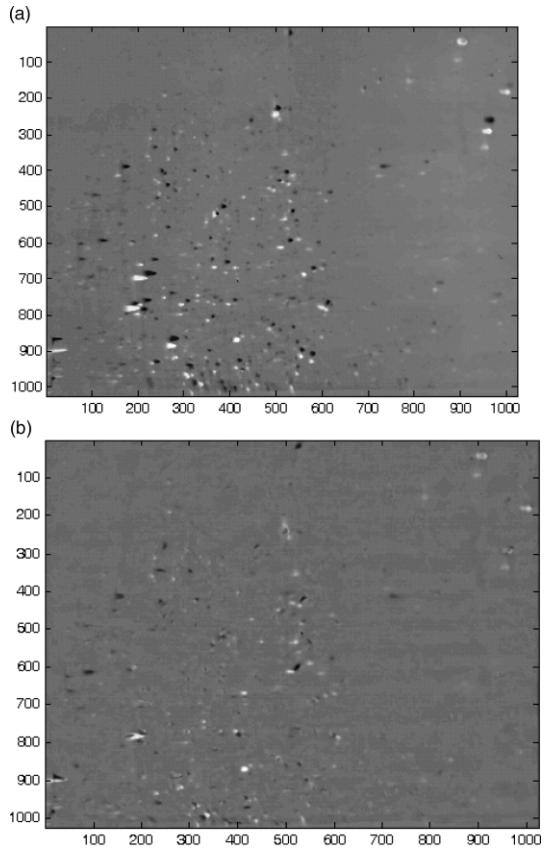

Fig. 12 Iterative registration of *S. coelicolor* gel images by the phase gradient method. (A) Difference between the original gels. The Euclidean distance between these gels is 540. (B) Final (5th iteration) registration. The Euclidean distance is now 370.

Registration to this degree is possible due to the cleanness of the original gels.

Caenorhabditis elegans

Next, the method is demonstrated on a very difficult registration problem with two *C. elegans* gel images (see ref. 91) with much streaking on the test gel. Once again the baseline is removed by median filtering and the resulting gel images are shown in Fig. 10.

This problem requires the resolving of multidirectional warping vectors across the test gel as indicated in Fig. 11a.

Using the same procedure as for both the above gel pairs produced a similar registration sequence. The difference between the reference and original test gel together with the movement map created by stage one of the phase gradient iteration, using scales 6,5,4,3 is shown in Fig. 11a. Again, the movement map at this iteration can be seen to follow the mismatched doublets quite well. Further iterations take the Euclidean Distance down through 254, 230 and 202 to produce the good final registration shown in Fig. 11b.

Streptomyces coelicolor

Especially following the completion of its genome sequence,[92] *S. coelicolor* proteome gels are currently of great interest,[93–95] so we include results (Fig. 12) for registering two 1024 × 1024 pixel images from *S. coelicolor* growth curves to a reference gel using the above method. These specific gels are from cultures of a mutant

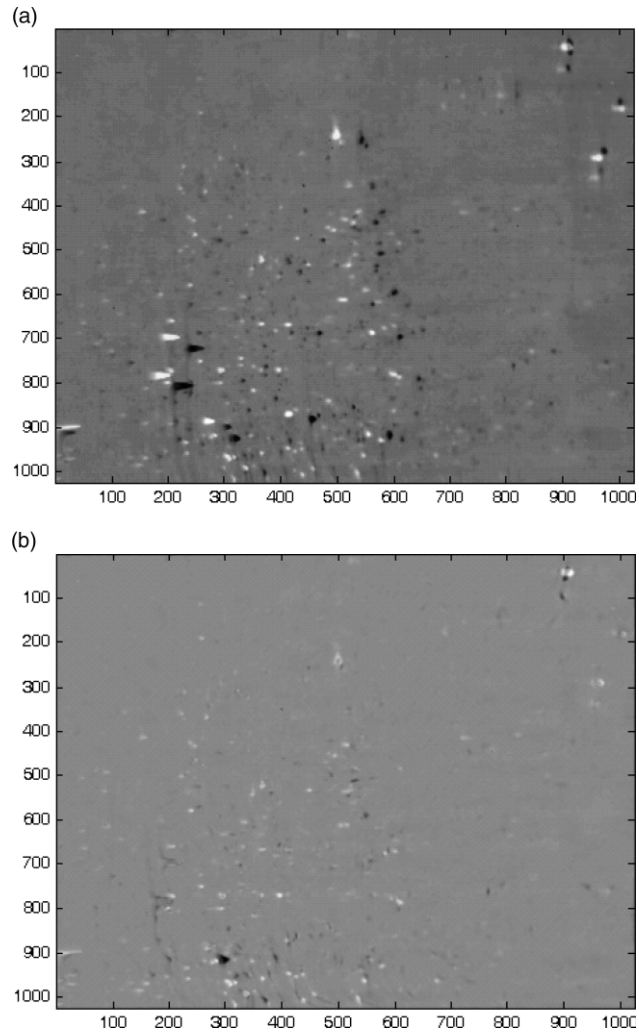

Fig. 13 Iterative registration of *S. coelicolor* gel images by the phase gradient method. (A) Difference between the original gels. The Euclidean distance between the gels is 650. (B) Final (5th iteration) registration; the Euclidean distance is now 400.

strain of M600 (M600 Δ*bldA*) grown in liquid culture in a minimal medium supplemented with casamino acids and sampled at 19 h and 36 h, respectively.

The algorithm can be seen to match spots warped in different directions across these gels very efficiently, dealing (especially in Fig 13) with quite large displacements, while preserving the significant differences between the gels. It is also notable in Fig 13 that due to its hierarchical nature dealing with gross movement first, then refining this estimate, the algorithm is able to resolve situations where the correct match for a particular spot is not the closest spot. This can probably be seen most clearly in the spot distribution around $x,y = 570,910$.

Conclusions

The QSWT-Warp method allows the rapid and robust automatic registration of a test image to a reference image, with no user input required during the process of setting or optimising control points. It deals with general warping functions both local and global, multi-directional warping vectors, and is applicable to any form of images. It is able to preserve real differences between the test image and the reference image since it merely warps the test image under the control of a complex wavelet transform but does not otherwise transform it. It is able to register precisely and efficiently using an iterative multiresolution approach, which is very fast on a modern PC. The typical speed-up relative to our previous automated registration routine based on evolutionary computing is approximately 1000-fold.

Acknowledgements

Thanks are due to the BBSRC for funding this project, to Nick Kingsbury (Cambridge University Engineering Department) for providing the QSWT software, to Bjørn Alsberg (Department of Chemistry, Norwegian University of Science and Technology) for initially drawing our attention to the DTWT, to Liz Davies (Dept. of Pharmacy, University of Brighton, now Dept. Chemistry UMIST), Jim Jefferies (Institute of Biological Sciences, University of Wales, Aberystwyth) and Andy Hesketh (John Innes Centre) for the *D. discoides*, *C. elegans* and *S. coelicolor* gel images respectively, and to Hailin Shen for assistance with file conversion and visualisation.

References

1 A. J. Link*2-D Proteome Analysis Protocols*Humana PressTotowaNJ1999.
2 M. Mann, R. C. Hendrickson and A. Pandey, *Annu. Rev. Biochem.*, 2001, **70**, 437–473.
3 R. Aebersold and M. Mann, *Nature*, 2003, **422**, 198–207.
4 M. Mann and A. Pandey, *Trends Biochem. Sci.*, 2001, **26**, 54–61.
5 R. Aebersold and M. Mann, *Nature*, 2003, **422**, 198–207.
6 C. A. Spibey, P. Jackson and K. Herick, *Electrophoresis*, 2001, **22**, 829–836.
7 R. Goodacre and D. B. Kell, *Anal. Chem.*, 1996, **68**, 271–280.
8 R. Goodacre, E. M. Timmins, A. Jones, D. B. Kell, J. Maddock, M. L. Heginbothom and J. T. Magee, *Anal. Chim. Acta*, 1997, **348**, 511–532.
9 J. S. Gustafsson, A. Blomberg and M. Rudemo, *Electrophoresis*, 2002, **23**, 1731–1744.
10 Z. Smilansky, *Electrophoresis*, 2001, **22**, 1616–1626.
11 S. Veeser, M. J. Dunn and G.-Z. Yang, *Proteomics*, 2001, **1**, 856–870.
12 A. M. Woodward, N. Kaderbhai, A. Shaw, J. Rowland and D. B. Kell, *Proteomics*, 2001, **1**, 1351–1358.
13 J. X. Yan, R. A. Harry, C. Spibey and M. J. Dunn, *Electrophoresis*, 2000, **21**, 3657–3665.
14 L. Dong and A. L. Boyer, *Int. J. Radiat. Oncol. Biol. Phys.*, 1995, **33**, 1053–1060.
15 B. Kim, J. L. Boes, K. A. Frey and C. R. Meyer, *Neuroimage*, 1997, **5**, 31–40.
16 N. Saeed, J. V. Hajnal, A. Oatridge and I. R. Young, *J. Mag. Res. Imaging*, 1998, **8**, 182–187.
17 H. Wu and Y. Kim, *Int. J. Imaging Syst. Technol.*, 1998, **9**, 29–37.
18 J. B. Maintz and M. A. Viergever, *Med. Image Anal.*, 1998, **2**, 1–36.
19 P. Gong, E. F. Ledrew and J. R. Miller, *Int. J. Remote Sensing*, 1992, **13**, 773–779.
20 N. Saeed, *NMR Biomed.*, 1988, **11**, 157–167.
21 J. Sato and R. Cipolla, *Image Vision Comput.*, 1995, **13**, 341–353.
22 G. J. Ettinger, G. G. Gordon, J. M. Goodson, S. S. Socransky and R. Williams, *J Clin. Periodontol.*, 1994, **21**, 540–543.
23 M. E. Alexander and R. L. Somorjai, *Magn. Reson. Imaging*, 1996, **14**, 453–468.
24 J. W. Hsieh, H. Y. M. Liao, K. C. Fan, M. T. Ko and Y. P. Hung, *Comput. Vision Image Understanding*, 1997, **67**, 112–130.
25 R. Sharman, J. M. Tyler and O. S. Pianykh, *Proc. SPIE*, 1997, **3078**, 497–505.
26 R. Adams and L. Bischof, *IEEE Trans PAMI*, 1994, **16**, 641–647.
27 A. Mehnert and P. Jackway, *Pattern Recognit. Lett.*, 1997, **18**, 1065–1071.
28 H. H. Li and Y. T. Zhou, *Opt. Eng.*, 1996, **35**, 391–400.
29 T. Gaens, F. Maes, D. van der Meulen and P. Suetens, *Lect. Notes Comput. Sci.*, 1998, **1496**, 1099–1106.
30 N. Hata, et al., *Lect. Notes Comput. Sci.*, 1996, **1131**, 317–326.
31 D. J. Hawkes, C. Studholme and D. L. Hill, *Radiology*, 1997, **205**, 111.
32 F. Maes, A. Collignon, D. van der Meulen, G. Marchal and P. Suetens, *IEEE Trans. Med. Imaging*, 1997, **16**, 187–198.
33 P. Viola and W. M. Wells, Alignment by maximisation of mutual information, *Int. J. Comput. Vision*, 1997, **24**, 137–154.
34 L. Thurfjell, Y. H. Lau, J. L. Andersson and B. F. Hutton, *Eur. J. Nucl. Med.*, 2000, **27**, 847–856.
35 D. Plattard, M. Soret, J. Troccaz, P. Vassal, J. Y. Giraud, G. Champleboux, X. Artignan and M. Bolla, *Comput. Aided Surg.*, 2000, **5**, 246–262.
36 J. P. Pluim, J. B. Maintz and M. A. Viergever, *IEEE Trans Med Imaging*, 2000, **19**, 809–814.
37 M. B. Skouson, Q. Guo and Z. P. Liang, *IEEE Trans Med Imaging*, 2001, **20**, 843–846.
38 T. D. Zuk and M. S. Atkins, *IEEE Trans. Med. Imaging*, 1996, **15**, 732–744.
39 K. Rohr, H. S. Stiehl, R. Sprengel, T. M. Buzug, J. Weesw and M. H. Kuhn, *IEEE Trans Med Imaging*, 2001, **20**, 526–534.
40 E. Bettens, P. Scheunders, D. Van Dyck, L. Moens and P. VanOsta, *Electrophoresis*, 1997, **18**, 792–798.
41 F. Meyer, A. Oliveras, P. Salembier and C. Vachier, *Ann. Telecommun.*, 1997, **52**, 367–379.
42 R. C. Gonzalez and R. E. Woods, *Digital Image Processing*, Addison-Wesley, Reading, MA, 1992.
43 K. P. Pleissner, F. Hoffmann, K. Kriegel, C. Wenk, S. Wegner, A. Sahlstrom, H. Oswald, H. Alt and E. Fleck, *Electrophoresis*, 1999, **20**, 755–765.
44 V. M. Bhajammanavar, K. C. Keong and S. M. Krishnan, *J. Digit. Imaging*, 2000, **13**, 127–129.
45 J. Montagnat and H. Delingette, *Lect. Notes Comput. Sci.*, 1997, **1205**, 13–22.
46 C. A. Glasbey and K. V. Mardia, *J. Appl. Stats.*, 1998, **25**, 155–171.
47 J. Ashburner, J. L. R. Andersson and K. J. Friston, *Neuroimage*, 1999, **9**, 619–628.
48 C. Davatzikos, *Comput. Vision Image Understanding*, 1997, **66**, 207–222.
49 P. Landau and E. Schwartz, *Graphical Mod. Image Proc.*, 1994, **56**, 247–266.
50 P. Chalermwat, in *Computational Science and Computer Engineering*, George Mason University, Fairfax, Virginia, USA, 1999.
51 J. J. Jacq and C. Roux, *Lect. Notes Comput. Sci.*, 1995, **905**, 205–221.
52 Y. Fan, T. Jiang and D. J. Evans, in *Evo Workshops 2002*, ed. S. Cagnoni, J. Gottlieb, E. Hart, M. Middendorf and G. R. Raidl, Springer Verlag, Heidelberg, 2002, **vol. LNCS2279**, pp. 304–314.
53 N. G. Kingsbury, in *IEEE Digital Signal Processing Workshop*, DSP 98 paper 86 Bryce Canyon, 1998.
54 N. G. Kingsbury, in *Proceedings of the European Signal Processing Conference*, EUSIPCO 98 319-322Rhodes; 1998.
55 N. G. Kingsbury, in *Proceedings of the IEEE Conference on Acoustics*, Speech and Signal Processing paper SPTM 3.6Phoenix, AZ; 1999.
56 N. G. Kingsbury, in *Phil. Trans. R. Soc. London Ser. A*, Discussion meeting on "Wavelets: the key to intermittent information?", London, 1999.

57 N. Kingsbury and J. Magarey, in *Proceedings of the First European Conference on Signal Analysis and Prediction*, Prague, 1997, pp. 23–34.
58 N. G. Kingsbury, in *Proceedings of the IEEE Colloquium on Time-Scale and Time-Frequency Analysis and Applications*, IEE London, 2000.
59 N. G. Kingsbury, in *Proceedings of the IEEE Conference on Image Processing*, Paper 1429, Vancouver, 2000.
60 N. G. Kingsbury, *Appl. Comput. Harmonic Anal.*, 2001, **10**, 234–253.
61 P. de Rivas, in *Engineering 233*, Cambridge, 2000.
62 J. Magarey and N. Kingsbury, in *Proceedings of the IEEE Conference on Image Processing*, 1996, pp. 969–972.
63 J. Magarey, A. Kokaram and N. Kingsbury, in *Proceedings of the IEEE Conference on Image Processing*, IEEE, Santa Barbara, 1997, pp. 187–190.
64 J. F. A. Magarey and N. G. Kingsbury, *IEEE Trans. Signal Proc.*, 1998, **46**, 1069–1084.
65 J. Magarey and A. Dick, in *Proceedings of the 14th International Conference on Pattern Recognition (ICPR '98)*, Brisbane, Australia, 1998, **vol. I**, pp. 4–7.
66 P. Loo and N. G. Kingsbury:, in *Proceedings of EUSIPCO 2000*, Tampere, Finland, 2000.
67 P. Loo and N. G. Kingsbury, in *Proceedings of the IEEE Colloquium on Secure Images and Image Authentication*, IEEE, London, 2000.
68 P. Loo and N. G. Kingsbury, in *Security and Watermarking of Multimedia Contents, Vol. SPIE Electronic Imaging*, San Jose, 2001, **vol. 4314**.
69 B. K. Alsberg, A. M. Woodward and D. B. Kell, *Chemom. Intell. Lab. Syst.*, 1997, **37**, 215–239.
70 A. N. Akansu and R. A. Haddad, *Multiresolution Signal Decomposition: Transforms, Subbands, and Wavelets*, Academic Press, New York, 1992.
71 I. Daubechies, *Ten Lectures on Wavelets*, SIAM, Philadelphia, 1992.
72 D. L. Donoho and I. M. Johnstone, *J. Am. Statist. Assoc.*, 1995, **90**, 1200–1224.
73 A. Grossmann, R. Kronland-Martinet and J. Morlet, *Reading and Understanding Continuous Wavelet Transforms, Wavelets: Time-Frequency Methods and Phase Space*, 1989, Springer-Verlag.
74 S. G. Mallat, *IEEE Trans. Pattern Anal. Machine Intell.*, 1989, **11**, 674–693.
75 M. Vetterli and Kovacevic, *Wavelets and Subband Coding*, Prentice Hall, Englewood Cliffs, NJ, 1995.
76 D. Casasent and R. Shenoy, *Proc. SPIE*, 1996, **2762**, 244–255.
77 H. G. Stark, *J. Math. Anal. Appl.*, 1992, **169**, 179–196.
78 J. Sadowsky, *Johns Hopkins APL Tech. Dig.*, 1994, **15**, 306–318.
79 A. V. Oppenheim and J. S. Lim, *Proc. IEEE*, 1981, **69**, 529–541.
80 P. de Rivas and N. Kingsbury, in *Proceedings of the IEEE Conference on Image Processing*, Kobe, Japan; 1999.
81 E. Davies, C. Olliff, I. Wright, A. Woodward and D. B. Kell, *Bioelectrochem. Bioenerg.*, 1999, **48**, 149–162.
82 Matlab, Edn. 6.1 Release 12, The Mathworks Inc., 14, Prime Par Way, Natick, USA; 2001.
83 Matlab Image processing toolbox user's guide, Edn. verision 3, 2001.
84 C. Gold, The Voronoi Website, http://www.voronoi.com/.
85 A. Okabe, B. Boots, K. Sugihara and S. N. Chiu, *Spatial Tessellations: Concepts and Applications of Voroni Diagrams*,, Wiley, Chichester, 2nd edn. 1999.
86 C. E. Shannon and W. Weaver, *The Mathematical Theory of Communication*, University of Illinois Press, Urbana, IL, 1949.
87 R. Battiti, *IEEE Trans. Neural Networks*, 1994, **5**, 537–550.
88 R. J. Gilbert, R. Goodacre, A. M. Woodward and D. B. Kell, *Anal. Chem.*, 1997, **69**, 4381–4389.
89 B. F. J. Manly, *Multivariate Statistical Methods : A Primer*, Chapman and Hall, London, 1994.
90 C. Chatfield and A. J. Collins, *Introduction to Multivariate Analysis*, Chapman and Hall, London, 1980).
91 J. Barrett, J. R. Jefferies and P. M. Brophy, *Parasitol. Today*, 2000, **16**, 400–403.
92 S. D. Bentley, K. F. Chater, A.-M. Cerdeno-Tarraga, G. L. Challis, N. R. Thomson, K. D. James, D. E. Harris, M. A. Quail, H. Kieser, D. Harper, A. Bateman, S. Brown, G. Chandra, C. W. Chen, M. Collins, A. Cronin, A. Fraser, A. Goble, J. Hidalgo, T. Hornsby, S. Howarth, C.-H. Huang, T. Kieser, L. Larke, L. Murphey, K. Oliver, S. O'Neil, E. Rabbinowitsch, M.-A. Rajandream, K. Rutherford, S. Rutter, K. Seeger, D. Sanders, S. Sharp, R. Squares, S. Squares, K. Taylor, T. Warren, A. Wietzorrek, J. Woodward, B. G. Barrell, J. Parkhill and D. A. Hopwood, *Nature*, 2002, **417**, 141–147.
93 J. Vohradsky, X. M. Li, G. Dale, M. Folcher, L. Nguyen, P. H. Viollier and C. J. Thompson, *J. Bacteriol.*, 2000, **182**, 4979–4986.
94 A. R. Hesketh, G. Chandra, A. D. Shaw, J. J. Rowland, D. B. Kell, M. J. Bibb and K. F. Chater, *Mol. Microbiol.*, 2002, **46**, 917–932.
95 J. Vohradsky, X. M. Li and C. J. Thompson, *Electrophoresis*, 1997, **18**, 1418–1428.